GIS-based Software Infrastructure to Model PV Generation in Fine-grained Spatio-temporal Domain

GIS-based Software Infrastructure to Model PV Generation in Fine-grained Spatio-temporal Domain

Lorenzo Bottaccioli, Edoardo Patti, Enrico Macii and Andrea Acquaviva.

***Abstract*—Nowadays, we are moving forward to more sustainable societies, where a crucial issue consists on reducing footprint and greenhouse emissions. This transition can be achieved by increasing the penetration of distributed renewable energy sources together with a smarter use of energy. To achieve it, new tools are needed to plan the deployment of such renewable systems by modelling variability and uncertainty of their generation profiles.**

In this paper, we present a distributed software infrastructure for modelling and simulating energy production of Photovoltaic (PV) systems in urban context. In its core, it performs simulations in a spatio-temporal domain exploiting Geographic Information Systems together with meteorological data to estimate Photovoltaic generation profiles in real operating conditions. This solution provides results in real-sky conditions with different time-intervals: i) yearly, ii) monthly and iii) sub-hourly. To evaluate the accuracy of our simulations, we tested the proposed software infrastructure in a real world case study. Finally, experimental results are presented and compared with real energy production data collected from PV systems deployed in the case study area.

***Index Terms*—Distributed Software Architecture, Geographic Information System, Solar Energy, Photovoltaic, Smart-city, Renewable energy sources.**

I. Introduction

DURING the international conference on climate changes (COP21) in 2015, the 196 parties attending the conference in Paris highlighted the need of reducing greenhouse gas emissions [1]. On this regard, in the last years, many countries are providing incentives to promote the deployment of low-carbon and sustainable technologies [2], such as Photovoltaic (PV) Systems. This implies both an increasing installation of Renewable Energy Sources (RES) and a smart use of energy in our cities [3]. Thus, specific tools to evaluate resource availability and uncertainty of RES are required: *i)* to understand their impact on power grids; *ii)* to perform load balancing; *iii)* to perform storage planning and management; *iv)* to perform demand-side management at different scales, from single user up to district or city; *v)* to provide generation profiles to electricity markets (e.g. day-ahead or intra-day market). By analysing the generation loads in fine-grained spatio-temporal domain (e.g. sub-hourly simulations of Photovoltaic systems at district scale), such tools should be able to overcome the current techniques estimating potential PV generation. The outcome of these tools is twofold. First, the impact on both power grids and electricity markets can be evaluated more accurately. Second, new policies for smart energy use can be developed. Information and Communication Technologies (ICT) have been identified as key player to foster this transition and to develop such innovative tools.

In particular, Geographic Information Systems (GIS) can become useful tools for planning renewable energy systems [4] in urban context and for evaluating their energy performances in spatio-temporal domain. In particular concerning PV systems, space and time domains must be considered to perform more accurate estimations of energy production [5]–[7]. Furthermore, the integration of these two domains helps to understand spatio-temporal dynamics in energy systems models [4], [8]. Literature solutions are limited in analysing solar potential in a spatial domain. Thus, they neglect temporal analysis (e.g. hourly or sub-hourly) to better model PV systems.

To overcome such limitations, we propose an innovative software infrastructure to estimate generation profiles of PV energy systems by performing fine-grained spatio-temporal simulations (e.g. 15-minutes simulations with a spatial resolution lower than $1\ m$). In its core, it computes real-sky conditions in urban context by simulating the incident radiation on tilted surface of buildings considering real meteorological data. Indeed, our solution integrates Volunteer Geographic Information (VGI) to exploit information available from personal weather stations [4].

Finally, we designed our infrastructure to ease the integration with third-party software that can exploit our results to develop tools for further analysis and evaluations (e.g. [9]–[12]).

Exploiting our software infrastructure, *Single citizen* can evaluate the economic and environmental savings achievable installing PV systems. *Energy aggregators and Energy Communities* can use simulation results to schedule consumption of their customers to maximize self-consumption. In particular, *Energy Communities* can exploit such infrastructure to perform feasibility studies and evaluate economic benefits [13]. *Energy managers* and *PV system engineers* can simulate the behaviour of their systems in real-sky conditions. This can help in sizing, validating and optimizing each system before and after the installation. *Distribution System Operators* (DSO) can take advantage of the proposed solution for network balancing and for planning retrofits and/or extensions of existing distribution grids. Finally, *Energy and City planners* can evaluate the impacts of large PV systems installations in city districts.

The rest of the paper is organized as follows. Section II reviews relevant background literature. Section III introduces the proposed software infrastructure to estimate PV energy production in urban contexts. Sections IV and V present respectively the case study and the experimental results. Finally, Section VI discusses concluding remarks and future works.

L. Bottaccioli, E. Patti, E. Macii and A. Acquaviva are with the Department of Control and Computer Engineering, Politecnico di Torino, Italy. Emails: {lorenzo.bottaccioli, edoardo.patti, enrico.macii, andrea.acquaviva}@polito.it

This work was partially supported by the EU project DIMMER (Grant Agreement no. 609084) and by the Italian project "Edifici a Zero Consumo Energetico in Distretti Urbani Intelligenti".

II. Related work

Geographic Information System (GIS) is considered useful tool to plan the deployment of renewable energy sources, such as solar, wind and biomass systems [4]. Particular emphasis is given to such technology for modelling solar potential in urban environments [8]. For example, the authors in [14] and [15] exploit GIS tools to estimate the yearly Photovoltaic (PV) potential starting from aerial and satellite images. Another approach consists in exploiting *Digital Surface Models* (DSMs) or 3D city models obtained from LiDAR data. DSM represents the earth's surface and includes all objects and buildings on it. For example starting from DSM, Hofierka et al. [16] estimated monthly and yearly solar potential in urban areas using *r.sun* tool [17]. While exploiting LiDAR data, Brito et al. [18] estimated yearly PV potential in Lisbon using ESRI *Solar Analyst* tool. These solutions just perform a time-domain analysis to estimate yearly solar potential. However, to provide more precise PV estimations, both space and time domains must be taken into account [5]–[7]. In [8] and [4], authors highlight that the integration of these two domains, with higher time and space resolutions, is needed to better understand spatio-temporal dynamics in energy systems models. This is required to *i)* plan deployment activities; *ii)* evaluate business plans; *iii)* monitor existing plants and *iv)* promote smart energy use.

On this premises, in order to provide simulation tools to wide range of users, GIS solutions have been developed exploiting a Web Service approach. Li et al. [19] have developed a service-oriented environment for sharing geoscience algorithms. They exploited both SOAP (Simple Object Access Protocol) technologies and OGC (Open Geospatial Consortium) standards to make available GRASS-GIS [20] features trough Web Services. *Gwass* [21] is a distributed web-based GIS built on top of the GeoBrain Web Services. This platform exploits a service-oriented architecture to offer an alternative to commercial desktop solution.

Literature provides also web-based solutions [22]–[29] to give PV energy potential information and to foster assessments of environmental and economic benefits as pointed out by Freitas et al. [8]. PVWatts [24] is a web application developed by the National Renewable Energy Laboratory that estimates yearly (Y), monthly (M) and hourly (H) PV production using a *Typical Meteorological Year* (TMY) and a topographic model of $40km^2$. PVGIS [22], [23] is a solar web map that offers information on yearly and monthly PV production in Europe and Africa. It provides also sub-hourly radiation information in clear-sky conditions. To perform this computations, it exploits *r.sun* starting form a DSM with a resolution of $1\ km$. i-Guess [26] is a web based system for urban energy planning in smart cities. It provides maps for yearly solar radiation on rooftops and for yearly PV potential. Mapwell Solar System [25] computes solar radiation and PV potential considering also a TMY.

It also provides information on rooftops and Region Of Interest (ROI). I-SCOPE [27] is an integrated platform to give 3-D smart-city services. In particular, it offers a solar map with Yearly and Monthly PV potential. Finally, Brumen et al. [28] developed a web application for PV potential assessments by exploiting *r.sun* starting from DSM. This platform provides data about yearly and monthly PV Potential together with information on rooftops and ROI. Such information on rooftops and ROI are also provided by I-SCOPE and i-GUESS services. Table I report the main features of the relevant literature solutions.

	Simulation Step			Sub-hourly Clear-sky simulation	Sub-hourly Real-sky simulation	Rooftop and/or ROI details	Weather Station data integration	Distributed and modular architecture	REST API
	Y	M	H						
Our Solution	✓	✓	✓	✓	✓	✓	✓	✓	✓
PVWatts [24]	✓	✓	✓						
PVGIS [23]	✓	✓		✓					
i-GUESS [26]	✓								
Mapdwell [25]	✓					✓			
I-SCOPE [27]	✓	✓				✓			
Brumen [28]	✓	✓				✓			

TABLE I
Comparison between the proposed architecture and relevant literature solutions

SAM [30] is another literature solution for PV modelling. It is a non-GIS tool that has been a standard for several years. It integrates third-party weather data (given as off-line files) to perform sub-hourly simulations. However, SAM does not simulate possible scenarios for PV deployment at urban scale that take into account surrounding buildings.

The main limitation of presented solutions consists on overlooking a fine-grained spatio-temporal domain in simulating and modelling energy production and performance of PV systems. Indeed, they are mainly focused on spatial domain by performing yearly or monthly simulations. On the other hand, existing spatio-temporal solutions perform hourly simulations with a low-resolution in spatial domain (e.g. resolution $> \ 1m$). To provide more accurate estimations, hourly and sub-hourly simulations with fine-grained resolution (e.g. DSM with resolution $< 1\ m$) are instead needed. This hight-resolution DSM allows to recognize and exclude encumbrance in rooftops, such as chimneys and dormers. Moreover, such simulations have to take into account real-sky conditions. To do so, they need real weather data (e.g. data from personal weather stations [4]) to compute incident radiation on tilted surface of rooftops and estimate PV performance and energy production.

As such, our contributions with respect to state-of-the-art, detailed in Table I, include the following: *i)* analysing together spatial and temporal domain in fine-grained resolution; *ii)* providing real-sky sub-hourly simulations, with 15-minutes time intervals; *iii)* integrating real meteorological data gathered from (personal) weather stations. Compared to current solutions that are monolithic software, we propose a distributed modular architecture based on a microservices approach [31], [32], where each module provides its Web Services to retrieve data. This approach eases the integration of our solution with third-party software and fosters the development of new services.

In our previous work [33], we provide a high-level description of the overall idea to develop a software infrastructure to model PV Generation in fine-grained spatio-temporal domain. With respect to [33], in this paper, we provide detailed description of the both methodologies *i)* to identify the suitable area where PV system can be installed and *ii)* to compute

the energy production of PV systems in real-sky conditions. In this paper, we also describe and compare the integrated decomposition models to estimate direct and diffuse solar radiation from the global solar radiation and how these have been applied to compute the incident radiation on pitched rooftops in real-sky conditions. Finally, we present the results about the extensive characterization we performed in a real-world case study carried out in Turin, Italy.

The results of the proposed solution can be conveniently applied to many contexts. For example, they can provide a better estimation of PV systems' impact on the power grids [34] as well as on the electricity market [10], [35]. In addition, they can be exploited to implement novel control policies for a smart energy usage, such as demand response.

III. Distributed software infrastructure to estimate PV energy production

In this work, we propose a distributed and modular software infrastructure that expose REST Web Services [36] to perform solar energy simulations (see Figure 1). Its modularity takes advantage of the microservices approach, which consists on developing software *as a suite of small services, each running in its own process and communicating with lightweight mechanisms* [31]. This increases flexibility and maintainability because services are *small, highly decoupled and focus on doing a small task* [32]. Our solution needs as main inputs the Digital Surface Models (DSMs) and the Cadastral maps. DSM is a raster image representing terrain elevation with buildings. A DSM with a high-resolution (in the order of sub-meters) permits i) to better recognize encumbrance in rooftops, such as chimneys and dormers, that would not allow deployment of PV panels and ii) to have a better simulation of shadows that will affect the PV energy production. Thus, higher is the DSM resolution, higher is the accuracy of the energy production estimation. Cadastral map is a vector image reporting the square footage of buildings in the area of interest. It also exploits meteorological data coming from third-party services to perform sub-hourly real-sky simulations of solar radiation and PV systems production. The main outputs are information on the size of deployable PV system(s) and the related generation profiles for each building that can be used as input to third-party solutions (e.g. [9]–[12]).

In addition, our solution exploits the standards defined by the Open Geospatial Consortium (OGC) [37], that specifies the interfaces for publishing and performing geospatial process over the web. In particular, it implements: *i)* Web Processing Services (WPS), *ii)* Web Feature Service (WFS) and *iii)* Web mapping Services (WMS). WPS are used for uploading both the DSM and the Cadastral map and for executing simulation processes. Indeed, they define rules for standardizing inputs and outputs of a process. WFS are used for querying and retrieving features about the elements of a polygon-map. WMS helps in visualizing the produced maps through the *Web-Map interface*. As shown in Figure 1, our solution is a three-layered distributed infrastructure consisting of: *i) Data-source Integration Layer*, *ii) Services Layer* and *iii) Application Layer*. The rest of this section describes each layer in more detail.

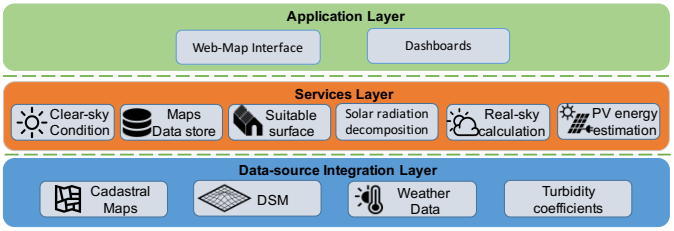

Fig. 1. Schema for the proposed software infrastructure to estimate PV energy production

Month	Jan	Feb	Mar	Apr	May	Jun	Jul	Aug	Sep	Oct	Nov	Dec
Date	17^{th}	16^{th}	16^{th}	15^{th}	15^{th}	11^{st}	17^{th}	16^{th}	15^{th}	15^{th}	14^{th}	10^{th}
DOY	17	47	75	105	135	162	198	228	258	288	318	344

TABLE II
Monthly average days identified by [42]

A. Data-source Integration Layer

The *Data-source Integration Layer* (the lowest layer in Figure 1) is in charge of integrating in the infrastructure the following heterogeneous information: *i) Digital Surface Model* (DSM); *ii) Cadastral map*; *iii) Linke Turbidity coefficients* [38] and *iv) Weather data*. The *Linke Turbidity coefficients* express the attenuation of solar radiation related to air pollution. This information can be automatically retrieved by third-party services, such as [23], [39], or can be specified by end-users before executing the simulation. Finally, *Weather data* are also retrieved by third party services, such as [40], and collected by personal weather stations deployed in cities. In particular, the needed inputs are solar radiation, ambient temperature and wind speed.

B. Services Layer for real-sky simulations

The *Services Layer* (the middle layer in Figure 1) is in charge of *i)* simulating solar radiation in real-sky condition; *ii)* identifying rooftops areas suitable for deploying PV systems and *iii)* evaluating their energy production. It consists of different software modules. It is worth highlighting that each of them exposes REST Web Services. Hence, each module can be invoked by third-party software to retrieve information and simulation results.

1) Clear-sky condition Service: In order to compute clear-sky solar radiation we exploit *GRASS-GIS* open-source software, which embeds in its core *r.sun* [17]. The *r.sun* tool provides an accurate simulation of solar radiation in urban contexts [8], [16], [41]. The resulting outputs of this module are set of direct and diffuse solar radiation maps in clear-sky condition with 15 minutes time interval. Such maps are stored in the *Maps Data-store* ready to be used by the *Real-sky calculation service*.

It performs such computation considering the monthly average days identified by [42] and reported in Table II with the related Day of the Year (DOY). DOY is a 1 to 365 non-dimensional sequential index starting from January 1^{st}. For instance: January 17^{th} is day 17, February 16^{th} is day 47, December 31^{st} is day 365.

The module requires as inputs: *i)* the DSM, *ii)* monthly *Linke* turbidity coefficients, *iii)* Slope and Aspect maps, that

are produced with *GRASS-GIS r.slope.aspect* tool. Monthly *Linke* turbidity coefficients are retrieved by using third party web services such as [23], [39] or can be specified by end-users as parameters in the execution request. The Slope and Aspect maps represent respectively the inclination and the orientation (expressed in degrees) of each pixel of the DSM. After their calculation, they are stored in the *Maps Data-store*.

2) Suitable surface identification service: Thanks to the high-resolution DSM given as input to the overall simulation process, this module identifies available surface for deploying solar systems on pitched rooftops excluding, for instance, dormers and chimneys. The *Suitable surface identification service* uses as inputs both Slope and Aspect maps for identifying the suitable area. These maps are retrieved from the *Maps Data-store*. By default, it identifies areas representing tilted rooftops oriented between South-Est and South-west. Commonly, a tilted rooftop has a slope (θ) in-between $10° \leq \theta \leq 45°$. This range is also suitable to install a PV system. Furthermore, facades with an orientation (γ) in-between $220° \leq \gamma \leq 320°$ (considering South facing roofs having $\gamma = 270°$) are more exposed to solar radiation. For these reasons, we chose these ranges for θ and γ as the default values for the *Suitable surface identification service*. However, the end-user can give as input new ranges for θ and γ to select the desired suitable surfaces.

The output of this selection is a binary map where pixels with 1 as value represent the available areas. Such map is then filtered with *GRASS-GIS r.neighbors* tool to smooth noise and to remove small areas that are too small for installing a PV system (e.g. areas where deployable PV system are smaller than 1 kW). This resulting map is vectorized and clipped with the cadastral map stored in *Maps Data-store*. The information on the size of area of the resulting polygons is a 2D projection of the real roof surface. To estimate the real surface of polygons, the Formula (1) is applied to correct the value of the area with inclination angle of rooftops.

$$S = \frac{S_{2D}}{cos(\theta)} \tag{1}$$

where S_{2D} is the 2D area of the polygon and θ is the roof inclination obtained from the slope map, again retrieved from the *Maps Data-store*.

The output of this module is a GeoJSON reporting a number of polygons that represent deployable areas.

3) Solar radiation decomposition service: Nowadays in our cities, weather stations are pervasively deployed and their information are also provided by third-party services, such as [40]. Normally such stations are equipped with global horizontal solar radiation sensors and do not provide information on direct normal and diffuse horizontal radiation. However, to simulate real-sky solar radiation on a pitched surface, information on direct and diffuse radiation is needed [17]. To overcome this limitation, the *Solar radiation decomposition services* integrates six different solar radiation decomposition techniques in literature [43]–[48] to compute both direct normal and diffuse horizontal radiation starting from measurements of global horizontal radiation.

These models can be categorized by the number of predictors. In the following we briefly introduce them. Erbs et al. [43], Reindl et al. [47] and Karatasou et al. [46] use only the clearness index k_t as predictor. k_t is the ratio between global radiation and extraterrestrial radiation both on a horizontal plane. Skartveit et al. [48] use k_t, solar altitude and solar zenith angles as predictors. Ruiz-Arias et al. [45] use k_t and the air mass as predictors. In their work, Engerer et al. [44] provide three different models. Our solution implements the second model with the following predictors: k_t, the zenith angle, the time of the day, the clear-sky global radiation on horizontal plane and a variability index, which represents the deviation of the observed k_t value from the clear sky value of the clearness index. The end-user can specify the model suitable for the area of interest. Indeed, as reported by [49]–[51], the accuracy of decomposition models is strongly affected by different latitude, longitude and environmental conditions. Hence, the integration of these decomposition models and third-party meteorological services makes our infrastructure flexible in performing simulation in different geographic locations. The input of this module is a time series of the global horizontal radiation provided by third-party meteorological services in *Data-source Integration Layer*. The output of this process is a JSON with the values of Direct Normal Incident radiation (DNI) and Diffuse Horizontal Incident radiation (DHI) for the requested time interval.

4) Real-sky calculation service: This module produces maps of incident global radiation on pitched rooftops in real-sky conditions. The inputs of this service are values of DNI, DHI, direct and diffuse solar radiation maps retrieved from the *Maps Data-store*. Through the *Data-source Integration layer*, the *Real-sky calculation service* retrieves information on solar radiation from third-party services. Both values of DNI and DHI radiation are required to calculate solar radiation on tilted surface [17]. If meteorological services provide only global horizontal radiation and not its direct and diffuse components, the *Real-sky calculation service* invokes the *Solar radiation decomposition services* to compute such information. Thus, *Real-sky calculation service* uses the values of DNI and DHI for each time interval to calculate the *clear-sky indexes* k_c^b (2) and k_c^d (3).

$$k_c^b = \frac{DNI_{overcast}}{DNI_{clear-sky}} \tag{2}$$

$$k_c^d = \frac{DHI_{overcast}}{DHI_{clear-sky}} \tag{3}$$

k_c^b (2) represents the ratio between DNI in overcast conditions and DNI in clear-sky conditions. While, k_c^d (3) is the ratio between DHI in overcast conditions and DHI in clear-sky conditions. Finally for each time interval, diffuse and direct radiation maps, produced by the *Clear-sky condition Service*, are multiplied by *clear-sky indexes* k_c^b and k_c^d. Then, both maps are summed together to obtain a global incident radiation map in real-sky condition. The resulting output of this process is a set of GeoTIFF images representing the maps with incident global solar radiation in real-sky condition.

5) Photovoltaic energy estimation service: This module is in charge of estimating PV production for each area identified by *Suitable surface identification service*. The required inputs are *i)* the maps provided by the *Real-sky calculation service* and *ii)* the GeoJSON given by the *Suitable surface identification service* where polygons representing deployable areas are

$$T_{sol-air} = T_a + k = T_a + \frac{\alpha_{roof}}{h_c} G_t \tag{4}$$

$$T_c = \frac{T_{sol-air} + (T_{c,NOCT} - T_{a,NOTC})(\frac{G_t}{G_{t,NOCT}})(1 - \frac{\eta_{mp,STC}(1-\alpha_p T_{c,STC})}{\tau\alpha})}{1 + (T_{c,NOCT} - T_{a,NOTC})(\frac{G_t}{G_{t,NOCT}})(\frac{\alpha_p T_{c,STC}}{\tau\alpha})} \tag{5}$$

$$T_c = \frac{U_{PV}(v) T_{sol-air} + G_t[\tau\alpha - \eta_{mp,STC}(1 - \alpha_p T_{c,STC})]}{U_{PV}(v) + \alpha_p \eta_{mp,STC} G_t} \tag{6}$$

$$U_{PV}(v) = 26.6 + 2.3v \tag{7}$$

$$P_{out} = \eta_{mp,STC}(1 + \alpha_p(T_c - T_{c,STC}))G_t A \tag{8}$$

T_a	ambient temperature	α_p	temperature coefficient of maximal power of the solar cells [%/°C]	$T_{c,STC}$	operating cell temperature at standard condition (usually $T_a = 25°C$, $G_t = 800\ W/m^2$)
α_{roof} [%]	convective factor of the roof	$\eta_{mp,STC}$	maximum power point efficiency under standard test conditions (%)	$G_{t,NOCT}$	solar radiation on a tilted surface at NOCT condition ($1000 W/m^2$)
h_c $[W/m^2K]$	radiative loss factor of the roof	τ	solar transmittance of any cover over the PV array (%)	U_{PV}	heat exchange coefficient for the total surface
G_t	solar radiation on a tilted surface	α	solar absorptance of the PV array (%)	A	available surface $[m^2]$
T_c	operating cell temperature	v	wind speed $[m/s]$		
$T_{c,NOCT}$	nominal operating cell temperature	P_{out}	power output $[W]$		

reported. The *Photovoltaic energy estimation service* also uses weather data coming from the *Data source integration layer* in order to estimate the operating cell temperature (T_c), thus the efficiency of the PV system. This module estimates from ambient temperature T_a the sol-air temperature $T_{sol-air}$ which is defined as the ambient Temperature T_a plus the loss factor k, as reported in Formula (4).

The use of sol-air temperature to obtain more reliable results in estimating the operating cell temperature is reported by [5], [6]. This module can use two models for estimating the cell temperature. The first [52], denoted as *NOCT*, can be used if wind speed is not provided by the nearest weather station. It is expressed by the Formula (5).

The second model [53], denoted as *Mattei*, uses wind speed in order to estimate the operating cell temperature, as reported in the Formula (6). *Mattei* model is one of the most reliable with in-situ wind data, as reported by [54].

In Formula (5), [42] assumes $\tau\alpha = 0.9$. While in Formula (6), [53] assumes $\tau\alpha = 0.81$. Finally, the instant power P_{out} is computed by Formula 8.

In its core, the *Photovoltaic estimation service* uses the characteristics of some commercial PV modules as default values (i.e. α_p, $\eta_{mp,STC}$, $T_{c,NOCT}$, $T_{c,STC}$, $G_{t,NOCT}$, α_{roof} and h_c). However before performing the simulation, the end-user can change this parameters depending on the characteristics of the interested PV system. The output of this module is a GeoJSON that provides for each building information on the size of deployable PV system and the related generation profiles for the requested time interval.

C. Application Layer

The *Application Layer* represents the highest layer of the proposed infrastructure (see Figure 1). It is dedicated to end-user applications, such as *Web-Map displayers* and *Dashboards*, that can provide information about performed simulation across the city with different level of details. In addition at this layer, third-party solutions can retrieve simulation results and estimations on PV energy production to perform further analysis and evaluations.

IV. Case Study

In order to test and validate the simulation of the proposed software infrastructure, we selected a district in Turin as case study. Turin is a city located in Piedmont, north-west of Italy. The district under analysis is *La Crocetta*, where there is our University campus. *La Crocetta* is located in the city centre with an area of about 3.7 km^2 and around 2200 residential buildings. It has been selected because of its buildings, which are heterogeneous for construction type and period. DSM and Cadastral maps for this area have been provided by the city council. DSM has a resolution of $0.25\ m^2$, which gives the possibility to describe with high accuracy rooftops, highlighting encumbrance like chimneys and dormers. Trough third-party web services, meteorological data (i.e. solar radiation and air temperature) are retrieved by the weather station in our University campus that is located in the middle of the case study district. The weather station collects global horizontal radiation by a *first class* pyranometer that samples every minute. Then, these samples are averaged and provided every 15 minutes. As proposed by [55], we exclude samples of solar radiation with: *i)* the altitude lower than 7° and *ii)* the clearness index lower than 0 and higher than 1. Furthermore, we excluded the measured samples of global horizontal radiation with higher values than in clear-sky condition, again as suggested by [55].

To validate our solution, we considered three different PV systems and a tilted solar radiometer located in the case study district. Thus, we compared results on PV energy simulation with real energy production data. The first PV system under analysis has been installed in our University campus (*Campus*) in 2008 with an inclination of 26° and an orientation of 23° (considering south 270°). It is a building integrated mono-crystalline system with an efficiency η_{pv} of 20.2% and a nominal power of $15.28\ kW$. The other two PV systems have been installed in 2004 in two public high

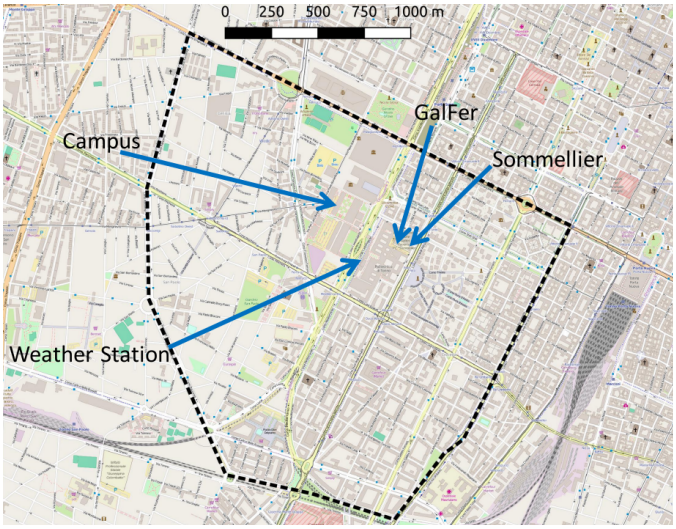

Fig. 2. Map of the case study district in Turin, Italy.

schools: *i) Istituto Galileo Ferraris* (*GalFer*) and *ii) Istituto Sommelier* (*Sommelier*). Both PV systems are poly-crystalline with a nominal power of 13.20 kW and 19.80 kW respectively and an efficiency of 13.1%. The $GalFer$ PV system is free-standing with an inclination of 35° and an orientation of 240°. The $Sommelier$ PV system is building integrated with an inclination of 20° and an orientation of 240°. Both GalFer and Sommelier have been monitored during the European project PERSIL [56] with whom we partially share the same case study. PERSIL aims at analysing the energetic performance of PV systems and solar thermal plants. Table III summarizes the characteristic of these three PV systems. Moreover, to validate the simulations of the *Real-sky calculation service*, we compared our results with measured data collected by a second solar radiometer, different from the one in the weather station. It is a mono-crystalline digital pyranometer and it is installed very closed to the PV system in our University campus. Figure 2 shows the case study area reporting the locations for the weather station and the three PV systems.

	Campus	GalFer	Sommelier
Nominal Power [kW]	15.28	13.20	19.80
Module Power [W]	283	165	165
Number of PV modules	54	80	120
Module Efficiency [%]	20.2	13.1	13.1
Module Temp. Coef. [%/°C]	0.38	0.48	0.48
Slope [°]	26	35	20
Aspect [°] (South 270°)	23	240	240
Installation year	2008	2004	2004

TABLE III
PV SYSTEM CHARACTERISTICS

V. EXPERIMENTAL RESULTS

In this section, we present the experimental results performed in the case study described in Section IV. First, we present the results achieved by the *Real-sky calculation service* compared with the real data collected by the digital pyranometer in our University campus. This test has been performed for all the solar radiation decomposition methods integrated in the proposed infrastructure in order to select the best method suitable for the case study area. Then, the resulting generation profiles, obtained by the *Photovoltaic energy estimation service*, are compared with measured data of *Campus*, *Sommellier* and *GalFer* PV systems. Finally to highlight the advantages of our solution, we performed simulations with one day time-interval for *Sommellier* and *GalFer* and we present the comparison of our simulation results with the simulation results obtained in PERSIL [56]. To evaluate the performance of our simulations, we exploited the indicators reported by Gueymard [57]. In particular, we considered the following four indicators of dispersion. *i)* The Mean Bias Difference (MBD) measures the average squares of errors between predicted and measured values. *ii)* The Root Mean Square Difference ($RMSD$) represents the standard deviation of differences between predicted and observed values. *iii)* The Mean Absolute Difference (MAD) is defined as the average of the absolute difference of two variables X and Y. *iv)* The Coefficient of determination (r^2) indicates the proportion between the variance and the predicted variable. These indicators of dispersion, with exception of r^2, are expressed in percentage of mean measured values rather than in absolute units as suggested in [57]. Furthermore, we considered the two following indicators for the overall performance. *i)* The Willmott's Index of Agreement (WIA) is the standardized measure of the degree of model prediction error. It varies between 0 and 1. *ii)* The Legates's Coefficient of Efficiency (LCE) is the ratio between the mean square error and the variance in the observed data, subtracted from unity. LCE can vary between $-\infty$ and 1, where 1 represents the perfect model.

A. Selection of best decomposition model for case study area

In order to select the best decomposition model for the case study area, all the models implemented in the infrastructure have been tested because their accuracy is strongly affected by the geographic location (see Section III-B3). The best model has been selected by comparing solar radiation simulations with measurements sampled by the solar radiometer in our University campus. The tests consisted on simulating solar radiation from the 1St of January 2014 to 31St of December 2015. Table IV reports the performance indicators of simulations for each decomposition model under analysis with time-intervals of 1 hour and 15 minutes respectively.

Model	Time resolution	LCE	MAD [%]	MBD [%]	r^2	$RMSD$ [%]	WIA
Reindl [47]	1 hour	0.80	15.38	-6.22	0.95	20.93	0.98
Engerer [44]		0.77	17.48	-5.96	0.93	24.16	0.98
Skartveit [48]		0.77	17.46	-8.62	0.93	24.10	0.98
Karatasou [46]		0.80	15.44	-1.88	0.95	20.73	0.98
Ruiz-Arias [45]		0.80	15.31	-0.68	0.94	20.75	0.98
Erbs [43]		0.80	15.47	-6.54	0.94	21.42	0.98
Reindl [47]	15 minutes	0.78	16.21	-6.08	0.93	23.52	0.98
Engerer [44]		0.75	19.09	-5.82	0.90	27.83	0.97
Skartveit [48]		0.75	18.75	-8.55	0.91	26.84	0.97
Karatasou [46]		0.78	16.57	-1.40	0.93	23.42	0.98
Ruiz-Arias [45]		0.78	16.65	-0.5	093	23.62	0.98
Erbs [43]		0.78	16.95	-6.36	0.93	24.35	0.98

TABLE IV
PERFORMANCE INDICATORS FOR SIMULATIONS OF SOLAR RADIATION

Period	Weather	LCE	MAD [%]	MBD [%]	r^2	$RMSD$ [%]	WIA
Winter	Sunny	0.75	14.29	-2.26	0.93	17.94	0.98
	Cloudy	0.75	17.17	-2.31	0.9	26.01	0.97
	Rainy	0.73	25.93	5.25	0.91	37.99	0.97
Spring	Sunny	0.8	13.14	-3.95	0.95	16.99	0.98
	Cloudy	0.79	15.01	-1.13	0.93	21.18	0.98
	Rainy	0.77	18.57	-0.38	0.93	30.72	0.97
Summer	Sunny	0.81	9.5	-4.39	0.96	11.91	0.98
	Cloudy	0.75	16.31	-3.01	0.91	21.79	0.97
	Rainy	0.71	22.6	-3.56	0.87	33.54	0.96
Autumn	Sunny	0.8	9.15	-0.13	0.95	12.06	0.98
	Cloudy	0.72	16.26	-1.66	0.9	21.01	0.96
	Rainy	0.71	24.63	6.73	0.91	32.81	0.99

TABLE V
PERFORMANCE INDICATORS FOR SIMULATIONS OF SOLAR RADIATION APPLYING KARATASOU MODEL [46]

The analysis of performance indicators for hourly simulations highlights that the best model for the case study area (Turin, Italy) is Karatasou [46]. Indeed, among its performance indicators, this model has the best values with exception of MBD, which is -1.88%. Indeed for MBD only, Karatasou is worst than the Ruiz-Aris model [45] with the $MBD = -0.68\%$. In 15 minutes simulation, Karatasou again has the best performance indicators with exception of MBD and MAD. Indeed, Ruiz-Aris achieves the best MBD, which is -0.5%; while Reindl [47] has the best MAD equal to 16.21%

Table IV highlights that all these decomposition models have better performance in simulation with 1 hour time-interval. This is also confirmed by Gueymard et al. [49], where authors proves that solar decomposition models developed to have the best performance with slow variations of k_t (e.g. hourly resolution) cannot provide same performance with faster variations of k_t (e.g. 15 minutes resolution).

Finally, Table V details the performance indicators for season and weather conditions (Sunny, Cloudy and Rainy) applying the Karatasou model [46]. Table V highlights that best results are achieved in sunny days of summer and autumn. Indeed for all seasons, MAD, MBD and $RMSD$ have lower values in sunny days. The r^2 is higher or equal to 0.9 for all seasons except for of rainy days in summer. On the other hand, simulations in winter season provide the worst results with respect to the other seasons, in particular during rainy days. More in general, rainy days for the fours seasons do not have the same good performance than in sunny days, with $RMSD$ higher than 30%. This is due to the accuracy of the integrated decomposition models in evaluating direct and diffuse components of solar radiation in rainy days. However, the results of 15-minutes simulations in rainy day (worst case) are still acceptable. We strongly believe that the exploiting sensors to sample direct and diffuse radiation will improve the performance of the simulations.

B. Evaluation of PV system simulation against measured data

In order to validate the estimation of generated instant power, we perform simulations for the three PV systems introduced in Section IV: *i) Campus*, *ii) Sommellier* and *iii) GalFer*. Then we compared our results with the real instant power sampled every 15 minutes. In our simulations for each PV system, we considered an yearly degradation factor of 1% for the efficiency

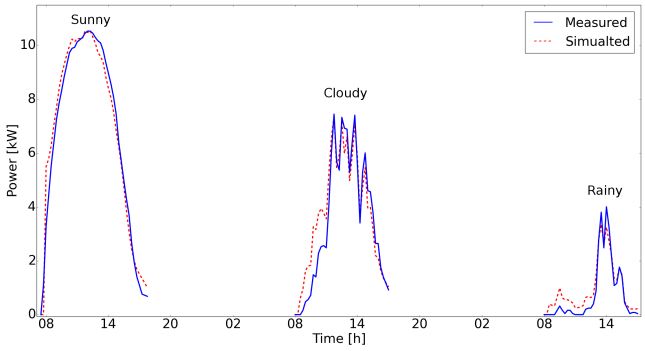

Fig. 3. Campus PV system generation loads for typical sunny, cloudy and rainy days.

Period	Weather	LCE	MAD [%]	MBD [%]	r^2	$RMSD$ [%]	WIA
Winter	Sunny	0.8	10.72	4.28	0.95	13.67	0.98
	Cloudy	0.77	15.7	6.59	0.93	20	0.98
	Rainy	0.66	33.13	17.5	0.89	41.87	0.96
Spring	Sunny	0.78	12.57	5.82	0.94	16.17	0.98
	Cloudy	0.74	18.27	2.13	0.9	25.29	0.97
	Rainy	0.73	21.69	2.07	0.9	30.72	0.97
Summer	Sunny	0.7	14.3	-0.94	0.89	18.04	0.97
	Cloudy	0.68	19.86	-1.86	0.86	26.02	0.96
	Rainy	0.66	26.2	-1.89	0.82	37.27	0.95
Autumn	Sunny	0.78	9.24	3.93	0.94	12.6	0.98
	Cloudy	0.7	16.91	3.82	0.89	22.09	0.97
	Rainy	0.67	28.85	13.35	0.89	36.94	0.97
18 months period for 15-min simulation	—	0.72	18.85	1.8	0.9	25.21	0.97
18 months period for daily simulation	—	0.82	9.64	7.93	0.96	11.68	0.99

TABLE VI
CAMPUS PERFORMANCE INDICATORS FOR OUR SOLUTION

coefficient η. For calculating the temperature $T_{sol-air}$, we set the loss factor k to 0.05 as reported by [5].

Figure 3 shows the comparisons among our results and measured generation load profiles for the *Campus* PV system in a time period from the 8^{Th} of May 2014 to the 31^{St} of December 2015. In particular, Figure 3 reports the plots of the instant power for three generic days in autumn: *i)* sunny, *ii)* cloudy and *iii)* rainy. It is worth noting that the trends of our results follow the real behaviour of the PV system with a good accuracy.

This is also highlighted by Table VI that reports the results in terms of performance indicators of instant power for the $Campus$ PV system. The best results are achieved in sunny days of autumn. Indeed, r^2 is higher than 0.9; $RMSD$ and MAD are respectively lower than 13% and 10%.

On the other hand, simulations performed in summer provide the worst results with respect to the other seasons, because the temperature strongly affects the efficiency coefficient η of the PV module.

Considering the whole time period (18 months), the accuracy of simulation performance for daily energy production increases with respect of 15 minutes time resolution. Daily simulations are computed as the integral of 15-minute simulations; thus, errors tend to be attenuated.

The other PV systems under analysis, both *Sommelier* and *GalFer*, have been monitored from the 1^{St} of March 2010 to the 22^{Nd} of February 2011 and the data sampling has been done by the PERSIL project consortium [56]. Table VII and VIII report the performance indicators of our simulation compared with

Time-frame	LCE	MAD [%]	MBD [%]	r^2	$RMSD$ [%]	WIA
15 minutes	0.7	21.42	14.38	0.87	28.29	0.97
Daily	0.76	11.64	9.81	0.94	14.63	0.98
Yearly	-	1.6	1.6	-	4.79	-

TABLE VII
SOMMELLIER SYSTEM PERFORMANCE INDICATORS FOR OUR SOLUTION

Time-frame	Interval	LCE	MAD [%]	MBD [%]	r^2	$RMSD$ [%]	WIA
15 minutes	All days	0.55	30.86	24.25	0.76	39.07	0.95
Daily	All days	0.5	14.97	54.25	0.78	28.05	0.95
Yearly	All days	-	2.69	2.69	-	8.08	-
15 minutes	Before 15/05/2010	0.78	15.99	7.94	0.92	23.09	0.981
15 minutes	After 15/05/2010	0.47	36.1	30	0.68	43.93	0.93
Daily	Before 15/05/2010	0.8	9.09	7.94	0.94	11.92	0.98
Daily	After 15/05/2010	0.4	30.55	29.99	0.71	32.71	0.94

TABLE VIII
GALFER SYSTEM PERFORMANCE INDICATORS FOR OUR SOLUTION

measured data for *Sommellier* and *GalFer* respectively. The simulations have been performed with different time-frames: *i)* 15 minutes, *ii)* 1 day and *iii)* 1 year. In both *Sommelier* and *Galfer*, the accuracy of performance indicators for simulations with daily and yearly time-frames increase with respect to 15 minutes simulations. LCE, WIA and r^2 are not calculated for yearly values because they can be applied to series and not to a single value. With respect to 15 minutes simulations, the accuracy of performance indicators for *Sommelier* simulations is in line with the one of *Campus*. Apparently, *GalFer* presents the worst accuracy. However, if the analysis is restricted to the period between 1St of March 2010 and 15Th of May 2010 the results are in line with the other PV systems. This is due to a malfunction of the PV system. Further details one this particular behaviour are discussed in next Section V-D

C. Comparison with PERSIL simulation methodology

During our studies and tests, we also compared our solution with PERSIL simulation methodology [56], with whom we partially share the same case study (i.e. *Sommellier* and *GalFer* PV systems). Figure 4 and Figure 5 show the real measured daily energy production compared with results of our solution and with results of PERSIL methodology for July 2010. Both Figures point out that PERSIL overestimates daily energy production with respect to our solution. In particular comparing PERSIL with our solution, $RMSD$ and MAD for *Sommellier* are 22.92% and 21.77% respectively. Regarding *GalFer*, it is worth noting that both solutions overestimate daily energy production due to the malfunction in the system occurred after the 15Th of May 2010 (see in Section V-D). However also in this case, our solution improves the estimations as show in Figure 5. Indeed comparing both methodologies, $RMSD$ and MAD for *GalFer* are 23.31% and 22.15% respectively. This is also highlighted and quantified by comparing the accuracy of performance indicators obtained by PERSIL in Table IX with ours in Table VII and VIII. This analysis underlines how our software infrastructure better describes the energy production with respect to PERSIL. Regarding the estimation of daily energy production for *Sommelier*, our solution reduces $RMSD$ of 32%, MBD of 28.88% and MAD of 24.34%. Considering the yearly energy production for the same PV system, our solution decreases $RMSD$ of 35.66%, both MAD and MBD of 35.79%. About the estimation of daily energy production for *GalFer* before the malfunction, our solution reduces $RMSD$ of 34.30%, MAD of 29.44% and MBD of 25.72%. Considering the yearly energy production for *GalFer*, our solution increases the accuracy by reducing the $RMSD$ of 42.79%, both MAD and MBD of 42.76%.

		LCE	MAD [%]	MBD [%]	r^2	$RMSD$ [%]	WIA
GalFer	Daily	-0.16	58.22	56.66	-0.22	66.26	0.8
	Daily (before 15/05/2010)	0.31	30.87	30.87	0.54	34.75	0.91
	Daily (after 15/05/2010)	-32	67.85	65.74	-0.55	76.01	0.78
	Yearly	-	6.29	6.29	-	18.88	-
Sommellier	Daily	0.183	40.3	40.3	0.386	45.6	0.88
	Yearly	-	4.47	4.47	-	13.43	-

TABLE IX
PERSIL PERFORMANCE INDICATOR FOR SOMMELLIER AND GALFER PV SYSTEMS

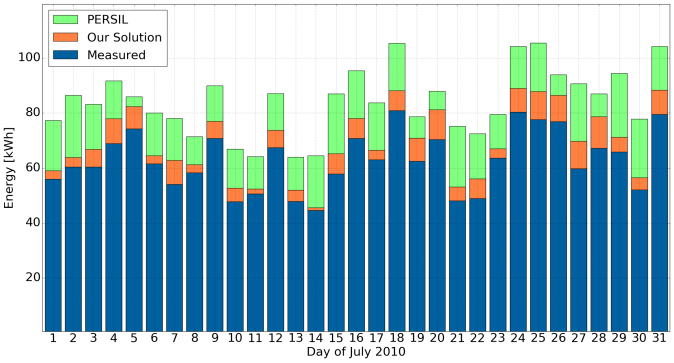

Fig. 4. Comparison of daily energy production of our simulation with measured data and PERSIL [56] (Sommelier PV system)

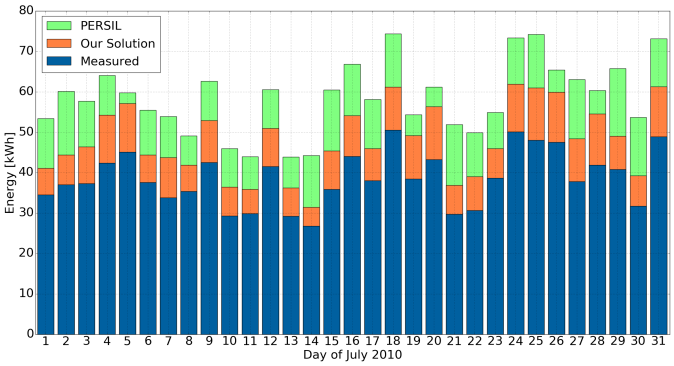

Fig. 5. Comparison of daily energy production of our simulation with measured data and PERSIL [56] (GalFer PV system)

In our case, the accuracy increases because our simulation process takes as inputs an high resolution DSM that is needed to simulate possible shadow behaviours. In addition, our solution consider $T_{sol-air}$ to better estimate the temperature for the PV cells. Finally, we computes the daily energy production as a sum of 15 minutes energy simulations. Thus, the effects of temperature on the PV efficiency is evaluated with real and actual values; while PERSIL exploits daily mean value.

D. PV system operation assessment

As mentioned in Section I, the proposed distributed software infrastructure can help *Energy managers* and *PV system engineers* in monitoring the performance of already deployed PV systems. This can help in planning maintenance activities

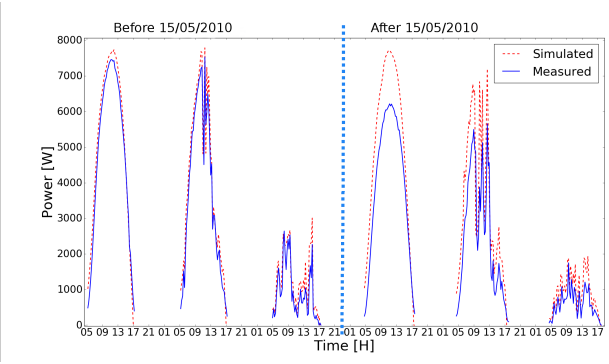

Fig. 6. Comparison of GalFer generation loads for Sunny, Cloud and Rain day before and after 15^{Th} of May 2010

by identifying systems that are not working properly. During our tests on *GalFer* and after a deep analysis of its generation loads, we identify a malfunction of the system that affects its performance from 15^{Th} of May 2010. Indeed, this anomaly decreases the efficiency of the modules reducing the maximum peak power. This is pointed out by analysing the peak power in a sunny day before and after 15^{Th} of May 2010. Indeed till 15^{Th} of May 2010, the simulation trends follow the real behaviour of the PV system. In particular, the peak power in 17^{Th} of May 2010 is $6354.77\ [W]$, with a global horizontal radiation of $844.10\ [W/m2]$ in sunny day. Instead, in 20^{Th} of April 2010, still a sunny day, the peak power is $7545.36\ [W]$ with a global horizontal radiation of $810.5\ [W/m2]$. This anomaly is also highlighted in Figure 6, where simulation results are compared with real measured values in sunny, cloudy and rainy days before and after 15^{Th} of May 2010. It is worth highlighting that this anomaly is not verified for *Sommellier*, which has almost the same system characteristics and geographic location of *GalFer* (see Section IV). Indeed, in the same days under analysis, the peak power is $10027.05\ [W]$ and $9937.60\ [W]$ respectively. In conclusion, we believe that results of the proposed solution can be used also to feed algorithms for detecting faults and/or malfunctions in PV systems.

VI. Conclusion and Future Works

In this work, we presented our distributed software infrastructure for modelling PV energy production in urban contexts. It overcomes the limitations of literature solutions by providing fine grained real-sky simulations considering also meteorological data from weather stations. Thus, addressing the challenges highlighted in [4]. Furthermore, the proposed solution performs simulations on spatial and temporal domains, providing energy profiles of PV systems with a good accuracy, as reported by the experimental results. Finally, our infrastructure can be use as a tool to help *Energy managers* and *PV system engineers* in monitoring the performances of existing PV systems as depicted in the analysed *GalFer* system, where a malfunction has been identified.

As future works, we will enhance the *Photovoltaic energy estimation service* by introducing detailed hardware models for the most relevant PV systems in the market. These hardware models are also needed to consider the effect of partial shading on PV systems.

References

[1] United Nations, FCCC, "Adoption of the Paris Agreement. Proposal by the President," 2015, Available: http://unfccc.int/resource/docs/2015/cop21/eng/l09r01.pdf.

[2] L. Dusonchet and E. Telaretti, "Economic analysis of different supporting policies for the production of electrical energy by solar photovoltaics in western european union countries," *Energy Policy*, vol. 38, no. 7, pp. 3297–3308, 2010.

[3] International Energy Agency., "Tracking clean energy progress 2016," 2016. [Online]. Available: http://www.iea.org/publications/freepublications/publication/TrackingCleanEnergyProgress2016.pdf

[4] B. Resch, G. Sagl, T. Törnros, A. Bachmaier, J.-B. Eggers, S. Herkel, S. Narmsara, and H. Gündra, "Gis-based planning and modeling for renewable energy: Challenges and future research avenues," *ISPRS International Journal of Geo-Information*, vol. 3, no. 2, pp. 662–692, 2014.

[5] L. R. Camargo, R. Zink, W. Dorner, and G. Stoeglehner, "Spatio-temporal modeling of roof-top photovoltaic panels for improved technical potential assessment and electricity peak load offsetting at the municipal scale," *Comput. Environ. Urban Syst.*, vol. 52, pp. 58–69, 2015.

[6] J. A. Jakubiec and C. F. Reinhart, "A method for predicting city-wide electricity gains from photovoltaic panels based on lidar and gis data combined with hourly daysim simulations," *Solar Energy*, vol. 93, pp. 127–143, 2013.

[7] N. Lukac, S. Seme, D. Zlaus, G. Stumberger, and B. Zalik, "Buildings roofs photovoltaic potential assessment based on lidar (light detection and ranging) data," *Energy*, vol. 66, pp. 598–609, 2014.

[8] S. Freitas, C. Catita, P. Redweik, and M. Brito, "Modelling solar potential in the urban environment: State-of-the-art review," *Renew. Sustainable Energy Rev.*, vol. 41, pp. 915–931, 2015.

[9] C. R. Hallam and C. Contreras, "Evaluation of the levelized cost of energy method for analyzing renewable energy systems: A case study of system equivalency crossover points under varying analysis assumptions," *Systems Journal, IEEE*, vol. 9, no. 1, pp. 199–208, 2015.

[10] J. Lin, "Potential impact of solar energy penetration on pjm electricity market," *Systems Journal, IEEE*, vol. 6, no. 2, pp. 205–212, 2012.

[11] C. Lavania, S. Rao, and E. Subrahmanian, "Reducing variation in solar energy supply through frequency domain analysis," *Systems Journal, IEEE*, vol. 6, no. 2, pp. 196–204, 2012.

[12] T. R. Ender, J. Murphy, and C. L. Haynes, "A framework for portfolio management of renewable hybrid energy sources," *IEEE Systems Journal*, vol. 4, no. 3, pp. 295–302, Sept 2010.

[13] L. Bottaccioli, E. Patti, A. Acquaviva, E. Macii, M. Jarre, and M. Noussan, "A tool-chain to foster a new business model for photovoltaic systems integration exploiting an energy community approach," in *Proc. of IEEE ETFA2015*. IEEE, 2015.

[14] L. Bergamasco and P. Asinari, "Scalable methodology for the photovoltaic solar energy potential assessment based on available roof surface area: further improvements by ortho-image analysis and application to turin (italy)," *Solar Energy*, vol. 85, no. 11, pp. 2741–2756, 2011.

[15] M. H. Kabir, W. Endlicher, and J. Jgermeyr, "Calculation of bright roof-tops for solar pv applications in dhaka megacity, bangladesh," *Renewable Energy*, vol. 35, no. 8, pp. 1760 – 1764, 2010.

[16] J. Hofierka and J. Kaňuk, "Assessment of photovoltaic potential in urban areas using open-source solar radiation tools," *Renewable Energy*, vol. 34, no. 10, pp. 2206–2214, 2009.

[17] M. Šúri and J. Hofierka, "A new gis-based solar radiation model and its application to photovoltaic assessments," *Transactions on GIS*, vol. 8, no. 2, pp. 175–190, 2004.

[18] M. C. Brito, N. Gomes, T. Santos, and J. A. Tenedório, "Photovoltaic potential in a lisbon suburb using lidar data," *Solar Energy*, vol. 86, no. 1, pp. 283–288, 2012.

[19] X. Li, L. Di, W. Han, P. Zhao, and U. Dadi, "Sharing geoscience algorithms in a web service-oriented environment (grass gis example)," *Computers & Geosciences*, vol. 36, no. 8, pp. 1060–1068, 2010.

[20] GRASS Development Team, *Geographic Resources Analysis Support System (GRASS GIS) Software*, Open Source Geospatial Foundation, USA, 2015. [Online]. Available: http://grass.osgeo.org

[21] F. Qiu, F. Ni, B. Chastain, H. Huang, P. Zhao, W. Han, and L. Di, "Gwass: Grass web application software system based on the geobrain web service," *Computers & Geosciences*, vol. 47, pp. 143–150, 2012.

[22] M. Suri, T. Huld, E. Dunlop, and T. Cebecauer, "Geographic aspects of photovoltaics in europe: contribution of the pvgis website," *J-STARS, IEEE Journal of*, vol. 1, no. 1, pp. 34–41, 2008.

[23] PVGIS. Http://re.jrc.ec.europa.eu/pvgis/apps4/pvest.php.

[24] B. Marion and M. Anderberg, "Pvwatts-an online performance calculator for grid-connected pv systems," in *Proceedings of the solar conference*. American Solar Energy Society; American Institute Of Architects, 2000, pp. 119–124.
[25] Mapdwell Solar System. Http://www.mapdwell.com.
[26] L. de Sousa, C. Eykamp, U. Leopold, O. Baume, and C. Braun, "iguess-a web based system integrating urban energy planning and assessment modelling for multi-scale spatial decision making," in *Porc. of iEMSs 2012*, 2012.
[27] R. De Amicis, G. Conti, D. Patti, M. Ford, and P. Elisei, *I-Scope-Interoperable Smart City Services through an Open Platform for Urban Ecosystems*. na, 2012.
[28] M. Brumenm, N. Lukac, and B. Zalik, "Gis application for solar potential estimation on buildings roofs," in *Proc. of WEB2014 International Conference on Building and Exploring Web Based Environments*. IARIA, 2015.
[29] L. Ménard, I. Blanc, D. Beloin-Saint-Pierre, B. Gschwind, L. Wald, P. Blanc, T. Ranchin, R. Hischier, S. Gianfranceschi, S. Smolders *et al.*, "Benefit of geoss interoperability in assessment of environmental impacts illustrated by the case of photovoltaic systems," *Selected Topics in Applied Earth Observations and Remote Sensing, IEEE Journal of*, vol. 5, no. 6, pp. 1722–1728, 2012.
[30] N. Blair, A. Dobos, J. Freeman, T. Neises, M. Wagner, T. Ferguson, P. Gilman, and S. Janzou, "System advisor model, sam 2014.1. 14: General description," 2014.
[31] M. Fowler and J. Lewis, "Microservices," 2014, Available: http://martinfowler.com/articles/microservices.html.
[32] S. Newman, *Building Microservices*. O'Reilly Media, Inc., 2015.
[33] L. Bottaccioli, E. Patti, M. Grosso, G. Rasconà, A. Marotta, S. Rinaudo, A. Acquaviva, and E. Macii, "Distributed software infrastructure for evaluating the integration of photovoltaic systems in urban districts," in *Proc. of the 5th International Conference on Smart Cities and Green ICT Systems (SMARTGREENS)*, 2016, pp. 357–362.
[34] L. Bottaccioli, A. Estebsari, E. Patti, E. Pons, and A. Acquaviva, "A novel integrated real-time simulation platform for assessing photovoltaic penetration impacts in smart grids," *Energy Procedia*, vol. 111, pp. 780–789, 2017.
[35] G. A. Pagani and M. Aiello, "Generating realistic dynamic prices and services for the smart grid," *Systems Journal, IEEE*, vol. 9, no. 1, pp. 191–198, 2015.
[36] R. T. Fielding and R. N. Taylor, "Principled design of the modern web architecture," *ACM Trans. Internet Technol.*, vol. 2, no. 2, pp. 115–150, May 2002.
[37] "Open Geospatial Consortium," Available: http://www.opengeospatial.org/.
[38] F. Linke, "Transmissions-koeffizient und trübungsfaktor," *Beitr. Phys. Fr. Atmos*, vol. 10, pp. 91–103, 1922.
[39] SoDa. Http://www.soda-is.com/.
[40] Weather Underground. Http://www.wunderground.com/.
[41] A. Ronzino, A. Osello, E. Patti, L. Bottaccioli, C. Danna, A. M. Lingua, A. Acquaviva, E. Macii, M. Grosso, G. Messina, and G. Rascon, "The energy efficiency management at urban scale by means of integrated modelling," in *Proc.of SEB-15*. Elsevier.
[42] J. A. Duffie and W. A. Beckman, *Solar Engineering of Thermal Processes*. Wiley, 2013.
[43] D. Erbs, S. Klein, and J. Duffie, "Estimation of the diffuse radiation fraction for hourly, daily and monthly-average global radiation," *Solar Energy*, vol. 28, no. 4, pp. 293–302, 1982.
[44] N. Engerer, "Minute resolution estimates of the diffuse fraction of global irradiance for southeastern australia," *Solar Energy*, vol. 116, pp. 215–237, 2015.
[45] J. Ruiz-Arias, H. Alsamamra, J. Tovar-Pescador, and D. Pozo-Vzquez, "Proposal of a regressive model for the hourly diffuse solar radiation under all sky conditions," *Energy Conversion and Management*, vol. 51, no. 5, pp. 881 – 893, 2010.
[46] S. Karatasou, M. Santamouris, and V. Geros, "Analysis of experimental data on diffuse solar radiation in athens, greece, for building applications," *International journal of sustainable energy*, vol. 23, no. 1-2, pp. 1–11, 2003.
[47] D. T. Reindl, W. A. Beckman, and J. A. Duffie, "Diffuse fraction correlations," *Solar energy*, vol. 45, no. 1, pp. 1–7, 1990.
[48] A. Skartveit and J. A. Olseth, "A model for the diffuse fraction of hourly global radiation," *Solar Energy*, vol. 38, no. 4, pp. 271–274, 1987.
[49] C. A. Gueymard and J. A. Ruiz-Arias, "Extensive worldwide validation and climate sensitivity analysis of direct irradiance predictions from 1-min global irradiance," *Solar Energy*, 2015.
[50] C. Jacovides, F. Tymvios, V. Assimakopoulos, and N. Kaltsounides, "Comparative study of various correlations in estimating hourly diffuse fraction of global solar radiation," *Renewable Energy*, vol. 31, no. 15, pp. 2492–2504, 2006.
[51] P. Ineichen, "Comparison and validation of three global-to-beam irradiance models against ground measurements," *Solar Energy*, vol. 82, no. 6, pp. 501–512, 2008.
[52] F. Brihmat and S. Mekhtoub, "Pv cell temperature/pv power output relationships homer methodology calculation," in *International Journal of Scientific Research & Engineering Technology*, vol. 1, no. 02. International Publisher &C. O, 2014.
[53] M. Mattei, G. Notton, C. Cristofari, M. Muselli, and P. Poggi, "Calculation of the polycrystalline pv module temperature using a simple method of energy balance," *Renewable energy*, vol. 31, no. 4, pp. 553–567, 2006.
[54] C. Schwingshackl, M. Petitta, J. E. Wagner, G. Belluardo, D. Moser, M. Castelli, M. Zebisch, and A. Tetzlaff, "Wind effect on pv module temperature: Analysis of different techniques for an accurate estimation," *Energy Procedia*, vol. 40, pp. 77–86, 2013.
[55] S. Younes, R. Claywell, and T. Muneer, "Quality control of solar radiation data: Present status and proposed new approaches," *Energy*, vol. 30, no. 9, pp. 1533 – 1549, 2005, measurement and Modelling of Solar Radiation and Daylight- Challenges for the 21st Century.
[56] F. Spertino and F. Corona, "Monitoring and checking of performance in photovoltaic plants: A tool for design, installation and maintenance of grid-connected systems," *Renewable Energy*, vol. 60, pp. 722 – 732, 2013.
[57] C. A. Gueymard, "A review of validation methodologies and statistical performance indicators for modeled solar radiation data: Towards a better bankability of solar projects," *Renewable and Sustainable Energy Reviews*, vol. 39, pp. 1024–1034, 2014.